Geochimica et Cosmochimica Acta, Vol. 69, No. 22, pp. 5279–5294, 2005

0016-7037/05 $30.00 + .00

doi:10.1016/j.gca.2005.07.001

Chemical weathering in the Upper Huang He (Yellow River) draining the eastern Qinghai-Tibet Plateau

Lingling Wu,[1] Youngsook Huh,[1,2,*] Jianhua Qin,[3] Gu Du,[3] and Suzan van Der Lee[1]

[1]Department of Geological Sciences, Northwestern University, 1850 Campus Drive, Evanston, Illinois 60208-2150 USA
[2]School of Earth and Environmental Sciences, Seoul National University, San 56-1, Sillim-dong, Gwanak-gu, Seoul 151-742, Korea
[3]Chengdu Institute of Geology and Mineral Resources, Chengdu, Sichuan 610082 P.R.C.

(*Received December* 17, 2004; *accepted in revised form July* 5, 2005)

Abstract—We examined the fluvial geochemistry of the Huang He (Yellow River) in its headwaters to determine natural chemical weathering rates on the northeastern Qinghai-Tibet Plateau, where anthropogenic impact is considered small. Qualitative treatment of the major element composition demonstrates the dominance of carbonate and evaporite dissolution. Most samples are supersaturated with respect to calcite, dolomite, and atmospheric CO_2 with moderate (0.710–0.715) $^{87}Sr/^{86}Sr$ ratios, while six out of 21 total samples have especially high concentrations of Na, Ca, Mg, Cl, and SO_4 from weathering of evaporites. We used inversion model calculations to apportion the total dissolved cations to rain-, evaporite-, carbonate-, and silicate-origin. The samples are either carbonate- or evaporite-dominated, but the relative contributions of the four sources vary widely among samples. Net CO_2 consumption rates by silicate weathering ($6–120 \times 10^3$ mol/km^2/yr) are low and have a relative uncertainty of ~40%. We extended the inversion model calculation to literature data for rivers draining orogenic zones worldwide. The Ganges-Brahmaputra draining the Himalayan front has higher CO_2 consumption rates ($110–570 \times 10^3$ mol/km^2/yr) and more radiogenic $^{87}Sr/^{86}Sr$ (0.715–1.24) than the Upper Huang He, but the rivers at higher latitudes are similar to or lower than the Upper Huang He in CO_2 uptake by silicate weathering. In these orogenic zones, silicate weathering rates are only weakly coupled with temperature and become independent of runoff above ~800 mm/yr.

1. INTRODUCTION

According to the uplift-weathering hypothesis of Raymo and Ruddiman (1992), the Cenozoic cooling of climate was caused by enhanced chemical weathering and consumption of atmospheric CO_2 in the mountainous regions of the world. The most prominent uplift in the last 40 to 50 Ma was in the Himalayas and the Tibetan Plateau (HTP) from collision of the Indian and Asian continents, and this area is still experiencing tectonism. Several large rivers—the Huang He (Yellow), Chang Jiang (Yangtze), Lancang Jiang (Mekong), Nu Jiang (Salween), Brahmaputra, Ganges, and Indus—arise from this "roof of the world" and present integrated information on chemical weathering at drainage basin scales. The Huang He, in its upper reaches, drains the northeastern portion of the Qinghai-Tibet Plateau (QTP), and the semiarid climate and lithology characterized by red beds, loess, and evaporite deposits differentiate this region from the Himalayan front that the Ganges-Brahmaputra system drains (Fig. 1a).

Previous studies of the fluvial geochemistry of the Huang He were conducted on the lower reaches suffering from severe anthropogenic impact (Carbon Cycle Research Unit, 1982; Hu et al., 1982; Gan et al., 1983; Zhang et al., 1990; Zhang et al., 1995). Our study focuses on the Upper Huang He above the city of Lanzhou (Fig. 1b). The region is sparsely populated, and cities with population above 1 million are limited to Lanzhou and Xining. Correspondingly, we expect the effect of city sewage and industrial waste to be smaller than in the lower reaches, where 15 high-population centers exist (Ministry of Public Security, 1993). The total sulfur deposition fluxes from combustion sources are also low (<50 mol/ha/yr) compared to eastern and southern China (250–2500 mol/ha/yr) (Larssen and Carmichael, 2000). This is because major centers of sulfur emission are Chongqing and Guiyang in the lowlands of southern China, and not only do the concentrations of SO_2 and SO_4^{2-} in the aerosols decrease significantly with elevation, but the center for sulfur deposition shifts to the east above 4 km due to the westerlies (Jiang et al., 1997). We thus presume acid rain to be inconsequential in the Upper Huang He. There are three dams (Longyang Xia, Liujia Xia, and Lijia Xia) above Lanzhou, and nine more downstream (Fig. 1b). The area irrigated for agriculture (wheat, maize, soybean) (Chen et al., 2003) accounts for less than 0.3% of the upper drainage basin compared to ~15% for the lower reaches (Yang et al., 2004). Hence, the saline irrigation return water will likewise be smaller in the Upper Huang He (Chen et al., 2003). There are two aluminum mines and one silver/gold mine in the Huang Shui drainage area; iron, zinc, copper, oil, and coal are more significant in the lower reaches (Hearn et al., 2001).

Our objective is to determine natural chemical fluxes above major point sources of anthropogenic contaminants and to examine chemical weathering rates in the periphery of the most prominent plateau under semiarid climate. We first present qualitative and quantitative estimates of the contribution of carbonate, evaporite, and silicate lithologies to the major element and strontium isotopic composition of the river-dissolved load. We then calculate the net CO_2 drawdown by silicate weathering. Comparisons are made to the Indus, Ganges, and Brahmaputra rivers draining the HTP (Pande et al., 1994; Galy

* Author to whom correspondence should be addressed (yhuh@snu.ac.kr).

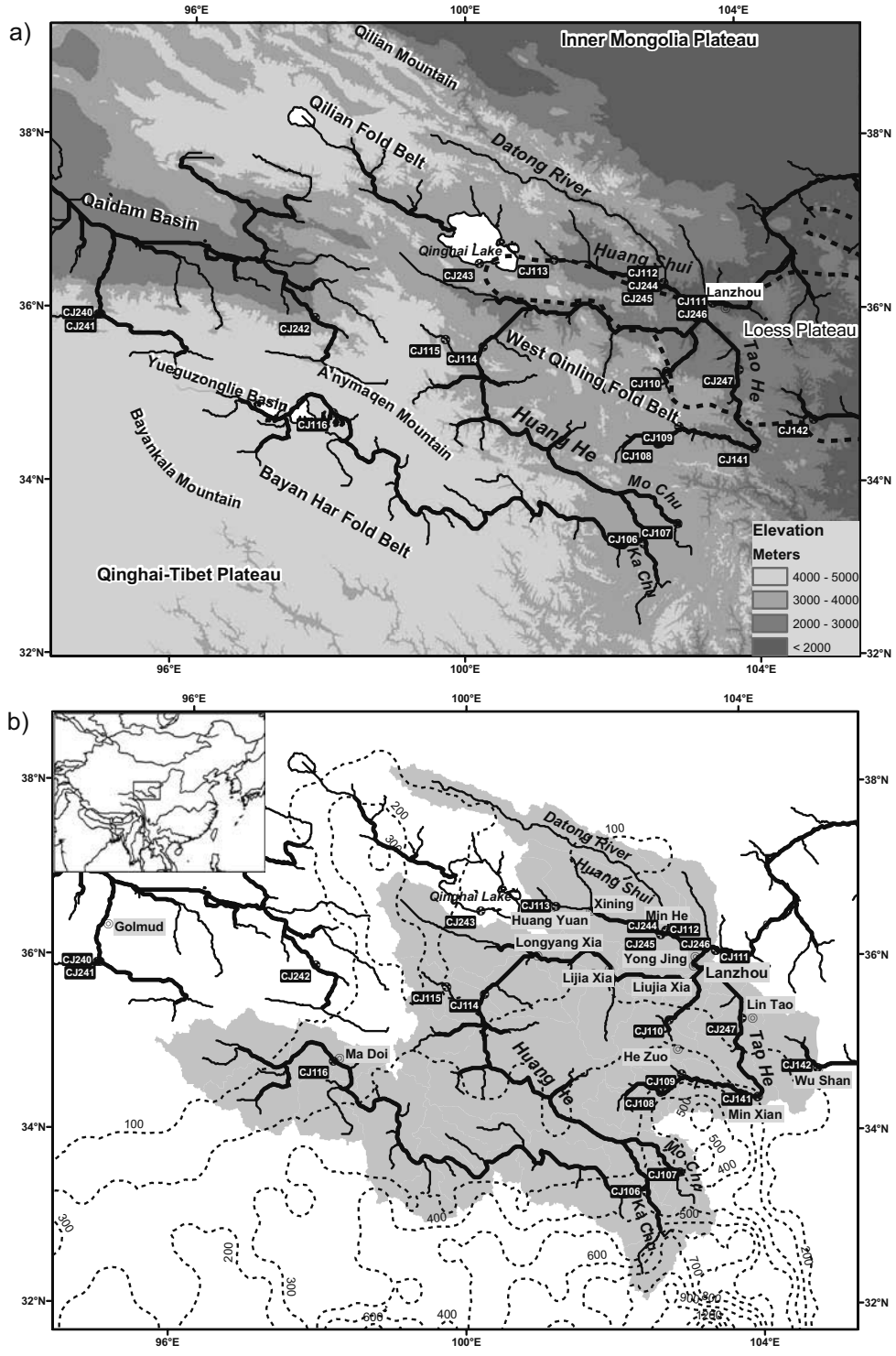

Fig. 1. (a) Elevation map of northeastern Qinghai-Tibet Plateau with sample locations, mountains, and major fold belts. The approximate boundary of the Loess Plateau is indicated with a dashed line (Sun et al., 2003). CJ100 and CJ200 series represent sample numbers for expeditions in 1999 and 2000, respectively. (b) Sample location map with runoff contours (in mm/yr) based on interpolated runoff from gauging station data (Fekete et al., 2002). The grey area is the Upper Huang He drainage basin above Lanzhou. Samples CJ240–242 lie outside it and are internally drained. Major cities and reservoirs are also shown.

and France-Lanord, 1999; Galy et al., 1999; Krishnaswami et al., 1999; Karim and Veizer, 2000; Dalai et al., 2002; Dalai et al., 2003) and to the Amazon, Orinoco, Mackenzie, Fraser, Yukon, Lena, Yana, Indigirka, and Kolyma, which drain major orogenic zones like the Andes, Rockies, and the Verkhoyansk and Cherskiy mountains (Stallard and Edmond, 1983; Cameron

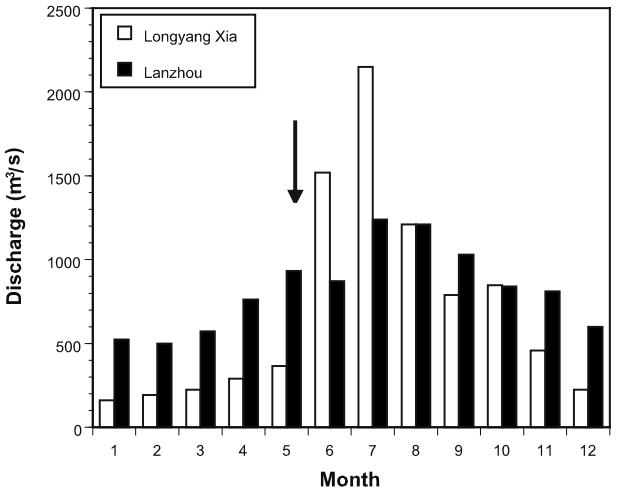

Fig. 2. The discharge of the Huang He at Longyang Xia station above the reservoir of the same name and at Lanzhou station (above downtown) from October 1998 to September 1999. The reservoir attenuates the large seasonal variation in discharge. Arrow indicates our sampling period.

et al., 1995; Edmond et al., 1996; Edmond and Huh, 1997; Huh et al., 1998a; Gaillardet et al., 2003; Millot et al., 2003). Unless otherwise specified, the data sets for the rivers that we discuss here are culled from the above references to include only the samples draining mountainous terrain. To make comparisons to the Huang He where we sampled during the rising stage (Fig. 2), we used the equivalent stage value where more than one season was sampled.

2. STUDY AREA

2.1. Geography

The Huang He ranks 26th in the world in terms of drainage area (0.752×10^6 km^2) and in sediment delivery is second only to the Amazon and similar to the Ganges-Brahmaputra system ($1{,}100 \times 10^6$ tons/yr; Meybeck and Ragu, 1997). It originates in the Yueguzonglie Basin on the Qinghai-Tibet Plateau (QTP) at an elevation of 4500 m, and the mean altitude of the Upper Huang He above Lanzhou is ~3,600 m (Fig. 1a). To the south, the Bayankala Mountain divides the Huang He and the Chang Jiang (Yangtze) drainage basins. In the north, the Qilian Mountain and the Huang Shui, the largest tributary on the Upper Huang He, mark the margin between the QTP and the Inner Mongolia Plateau (Fig. 1a). The Tao He, the second largest tributary, drains northeastern QTP and western Loess Plateau. The Qinghai Lake formed in the Pliocene and has been a closed basin lake (no river outlet) since 36 Ka (Yan et al., 2002). The mean local relief (the "maximum-minimum" elevation within each 10-min grid cell) of the Upper Huang He is 1600 m, while that of the entire basin is 461 m (Summerfield and Hulton, 1994).

2.2. Geology

We will describe below the geology of the samples relative to the three major fold belts—the Bayan Har, West Qinling, and Qilian. The source waters of the Huang He (sample number: CJ116) drain the western Bayan Har Fold Belt, of Indosinian (late Triassic) age, composed of sandstone, dolomitic limestone, and minor volcanic rocks (Yang et al., 1986) (Fig. 1a). Thin-bedded halite deposits are also found in the area (Zheng, 1997). Two tributaries, Ka Chu (CJ106) and Mo Chu (CJ107), drain the eastern Bayan Har Fold Belt, made up of Quaternary fluvial sandy slate, limestone, and granite (Zheng, 1997). The Tao He tributary drains the West Qinling Fold Belt of Indosinian age with sandstone, slate, limestone, and locally Tertiary evaporite-bearing red beds, Quaternary gypsiferous lacustrine deposits, and granite (Yang et al., 1986; Zheng, 1997). The Huang Shui tributary drains the Qilian Fold Belt of Caledonian (Cambrian to Silurian) age, which has been reactivated by the collision between India and Asia (Tapponnier et al., 1986). Proterozoic to Lower Paleozoic metamorphic rocks and granite, locally Triassic sandy slate with limestone, and Tertiary sandstone, mudstone, and gypsum are exposed (Zheng, 1997). Massive Caledonian volcanogenic sulfide deposits composed of pyrite (FeS_2), chalcopyrite ($CuFeS_2$), galena (PbS), and sphalerite (ZnS) occur in the northern Qilian Fold Belt (Sun, 1992). Three samples are from outside the Huang He drainage basin proper and are internally drained into the Qaidam Basin, where halite, mirabilite ($Na_2SO_4 \cdot 10H_2O$), borax ($Na_2B_4O_7 \cdot 10H_2O$), sylvite (KCl), and bischofite ($MgCl_2 \cdot 6H_2O$) are exposed (Yang, 1989; Vengosh et al., 1995; Zheng, 1997). Loess is widely distributed in northern China (Sun, 2002), and the Huang Shui tributaries, the mainstream at Lanzhou, and some Tao He tributaries drain loess-covered areas (Fig. 1a).

2.3. Climate, Hydrology, and Vegetation

The East Asia-West North Pacific subsystem of the Asian-Australian monsoon affects the Upper Huang He basin (Wang et al., 2003). In winter, the high pressure over Mongolia dominates, northerlies prevail, and the climate is dry (~100 mm precipitation) and cold (average winter air temperature −11°C; Wang and Lin, 2002; Wang et al., 2004). In summer, the subtropical high pressure of the west Pacific becomes strong, with warm (average summer air temperature of 11°C), wet (~400 mm) air masses entering the Tibetan Plateau and gradually displacing the Mongolian high. The meeting of cold and warm air masses brings large amounts of rainfall, and May to September is the rainy season. Annual precipitation is ~430 mm on average for the period 1950–1999 in the Upper Huang He (Wang et al., 2002). For the last 50 yr, precipitation has been on a decreasing trend, especially since the 1990s, resulting in lower runoff (Wang et al., 2004). The annual potential evapotranspiration is ~1400 mm and has been increasing at a rate of 3.25 mm/yr since the 1980s, with the air temperature increasing 0.4°C per decade (Li et al., 2000; Yang et al., 2004).

Satellite images show that the snow cover is distributed primarily above 4000 m in the A'nymaqen Mountain from early October to mid-April, and the snow line rises to around 4700 m in late May (Fig. 1a; Lan et al., 1999). Snowmelt flood, together with the increase in precipitation, leads to the abrupt rise of the river runoff in June (Fig. 2). In the case of Longyang Xia station, June to September generates most of the year's discharge, whereas at Lanzhou station dams attenuate the sea-

sonal variation. The natural discharge recorded at Lanzhou station for the period 1990 to 1999 has declined by 16% relative to the 50-yr average (33.6 km^3/yr), due to decreased precipitation and increased evapotranspiration (Wang et al., 2002).

The headwaters of the Huang He and its tributaries (CJ116, 106, 107) flow through largely grassland and woodland with minor mountain, glacier, desert, and swampland; tillage land is minimal (Han, 2002). The alpine shrub and meadows are major vegetation types, with pockets of conifer forests on the northern slopes of the Qilian Mountain range (Wen et al., 2004). The vegetation cover in the headwater catchments (above CJ116) of the Huang He has decreased, at most 0.3% per yr over the last 20 yr (Yang et al., 2002), due to the degradation of permafrost and subsequent lowering of the groundwater table (Peng et al., 2003; Zhang et al., 2004).

3. SAMPLING AND ANALYTICAL METHODS

Sampling expeditions were made in May–June of 1999 and June of 2000, during the rising stage (Fig. 2). Samples for major elements were filtered through 0.45 μm cellulose acetate filters, and those for Sr through 0.4 μm polycarbonate filters in the field within 24 h of collection. Samples for Si and Sr were acidified with ultrapure HNO_3 and stored in precleaned HDPE bottles. The pH was measured at the time of sampling to ensure against CO_2 loss. Major cations (K, Na, Ca, Mg) were analyzed by flame atomic absorption spectrometry, alkalinity by Gran titration, Cl^- and SO_4^{2-} by ion chromatography, and silica by colorimetry. Strontium concentrations were determined by inductively coupled plasma-mass spectrometry (ICP-MS) and $^{87}Sr/^{86}Sr$ by thermal ionization mass spectrometry (TIMS) (Finnigan MAT251, U.S. Geological Survey, Menlo Park, CA). The long-term value for NBS987 was 0.71023 $\pm$ 0.00002.

4. RESULTS AND DISCUSSION

4.1. Major Elements and Strontium

The river waters sampled are alkaline, with pH values greater than ~8 (Table 1). The total dissolved cations ($TZ^+ = Na^+ + K^+ + 2Mg^{2+} + 2Ca^{2+}$ in μEq = 10^{-6} charge equivalent units per liter) and total dissolved anions ($TZ^- = Cl^- + 2SO_4^{2-} + HCO_3^-$ in μEq) balance within $\pm$8% (net inorganic charge balance, NICB in Table 1). Six high-TDS (total dissolved solid) samples—the Qinghai Lake, internally drained rivers, lowermost Huang Shui (CJ245), and Wei He (CJ142) —have exceptionally high TZ^+ of 6,500 to 258,000 μEq. For others, the TZ^+ values range from 1000 to 6000 μEq (Table 1), still higher than the average for world rivers (TZ^+ ~1,250 μEq) (Meybeck, 1979) or rivers in other orogenic zones (several hundred to ~3,000 μEq).

The major element composition indicates qualitatively that carbonate and evaporite weathering is significant and that silicate weathering is a minor source of the dissolved load (Fig. 3). The uppermost Huang He (CJ116), internal drainage samples, and the Qinghai Lake are dominated by Na, and to a lesser extent, Mg (Na > Mg > Ca > K) (Table 1). The Huang He at Lanzhou, lowermost Huang Shui (CJ245), and Wei He (CJ142) are also high in Na, but their Mg content is not very high (Na > Ca > Mg > K). Calcium is the dominant cation in the rest of the samples (Ca > Mg > Na > K). Relative concentrations of (Na + K) are highly variable among samples, but Mg levels are more steady (Fig. 3a). The high-TDS rivers have high proportions of Cl and SO_4, while bicarbonate (HCO_3^-) dominates the anions in nonhigh-TDS samples (Fig. 3b; Table 1). Dissolved silica, SiO_2(aq), contributes less than 10% of the anions and is especially low in the Qinghai Lake sample. Only in the Ka Chu and Mo Chu (CJ106, 107) is silica significant.

In the Huang He, the major ion concentrations increase progressively from southern headwater tributaries (CJ106, 107) north to Lanzhou (Table 1; Fig. 1b). Stable isotope ratios, $\delta^{18}O$ and δD, show a similar trend (Su et al., 2001), suggesting that there is more evaporation northward. The source sample (CJ116) in the west is more concentrated, consistent with the lower runoff values there (Fig. 1b). Huang He at Lanzhou (CJ111, CJ246) and Datong He at Min He (CJ112, CJ244) sampled in two consecutive years have interannual variability within 10% for the dominant ions Ca and HCO_3, and within 5% TDS (Table 1).

4.1.1. *Evaporite dissolution and sulfide oxidation*

The Cl concentrations are extremely high (>~2000 μM) for the high-TDS samples, but still in the hundreds of μM range for most other samples. Only the headwater tributaries (CJ106, 107) and Tao He tributaries have lower concentrations. Considering that the Upper Huang He is remote from marine influence, evaporite dissolution likely overwhelms input from marine aerosol. The slight Na excess above the halite equivalence (Na:Cl = 1:1) may be from other Na-containing salts like borax (especially in the internal drainage) or from weathering of albite and Na-containing clays in clastic rocks (Table 1). Sodium and chloride are the main constituents of the Qinghai Lake, in accordance with what has been reported in the literature (Na-Mg-Cl-SO_4 type brine; Yan et al., 2002; Jones and Deocampo, 2003).

Three potential sources of sulfate in rivers are (1) gypsum, (2) pyrite, and (3) pollution from coal combustion. Distinguishing between these sources is important for the CO_2 budget because the latter two can generate H^+ and thus allow silicates and carbonates to weather without consuming atmospheric CO_2. In the high-TDS rivers, the near equivalence of Ca and SO_4 suggests that gypsum is the source, but the high Cl/SO_4 ratios (except CJ245 and CJ116) indicate that halite and other minor chloride salts $MgCl_2$ and KCl remain significant. For nonhigh-TDS samples, the Cl and SO_4 are comparable and lower in concentration than the high-TDS samples (Table 1). The volcanogenic deposits in the Huang Shui drainage area (Sun, 1992) and oxidation of pyrite (FeS_2) might contribute SO_4 to these tributaries, but it is difficult to quantify this using only the major element concentrations. Sulfur and oxygen isotope ratios of SO_4 may separate these two sources (Calmels et al., 2004). The source of SO_4 from pollution is considered to be minor in the study area because the fluxes of sulfur emission and deposition are low (see section 1).

We computed the gypsum saturation index (GSI) using the Geochemist's Workbench v.4.0 (Bethke, 2002) and the thermodynamic database provided with the program. GSI is defined as $\log(\{Ca^{2+}\}\{SO_4^{2-}\}/K_{gypsum})$ where {} denotes activity. All samples are undersaturated with respect to gypsum (GSI −3.8 to −1.2), with the Ka Chu (CJ106) and Mo Chu (CJ107) most undersaturated and the high-TDS samples least undersaturated.

Table 1. The chemical composition of the dissolved load for the Upper Huang He and internal drainage rivers.

River name[a]	Sample No.	Date mm/dd/yy	Elevation[b] m	pH	T °C	Na μM	K μM	Mg μM	Ca μM	Cl μM	SO_4 μM	Alk μEq	Si μM	TDS[c] mg/l	TZ^{+}[d] μEq	NICB[e] %	Sr μM	$^{87}Sr/^{86}Sr$
Huang He																		
Huang He @ Ma Doi	CJ116	06/02/99	4490	8.89	2.8	2090	65.6	946	849	1835	210	3327	26.2	394	5746	2.8	5.40	0.71044
Ka Chu @ Tang Ku	CJ106	05/29/99	3740	8.27	11.0	127	16.3	90.5	349	21.5	24.3	891	111	83.0	1022	6.0	1.10	0.71111
Mo Chu @ Roergai	CJ107	05/30/99	3577	8.22	10.4	147	23.9	113	443	24.4	19.5	1128	120	102	1283	7.1	1.17	0.71096
LB trib. of Huang He	CJ115	06/01/99	4331	8.84	6.6	402	32.1	330	1330	281	493	2228	97.5	269	3754	6.9	3.40	0.71134
Huang He bl. Tangnag	CJ114	06/01/99	4110	8.83	11.7	274	28.2	397	936	115	110	2489	96.2	224	2968	4.9	3.35	0.71100
RB trib. of Huang He	CJ110	05/30/99	3413	8.94	9.9	532	46.6	810	756	242	330	2808	74.1	277	3711	0.0	6.48	0.71099
Huang He @ Lanzhou	CJ111	05/31/99	3648	8.60	13.1	1630	48.8	682	1210	1010	532	3044	105	380	5463	6.3	6.16	0.71142
Huang He @ Lanzhou	CJ246	06/20/00	3648	8.33	19.5	1715	58.1	722	1200	951	660	2889	113	385	5617	8.1	7.38	0.71117
Wei He @ Wu Shan	CJ142	06/15/99	2323	8.54	16.8	4435	96.4	1320	1700	4290	1700	3062	111	712	10570	−1.7	9.88	0.71097
Tao He Tributary																		
Tao He headwaters	CJ108	05/30/99	3653	8.86	6.8	168	24.2	609	605	66.0	60.0	2459	96.4	205	2620	−0.9	4.00	0.71019
LB trib. of Tao He	CJ109	05/30/99	3402	8.92	6.5	220	28.0	495	695	80.5	66.2	2396	76.5	204	2628	0.7	4.40	0.71151
Tao He @ Min Xian	CJ141	06/14/99	3444	8.93	18.1	172	30.3	503	1130	83.8	99.7	3085	72.1	263	3468	2.9	4.78	0.71075
Tao He ab. Lin Tao	CJ247	06/21/00	3272	8.25	23.7	333	52.6	562	1130	109	194	3016	86.8	277	3770	6.8	5.50	0.71093
Huang Shui Tributary																		
Datong He @ Min He	CJ112	05/31/99	3504	8.73	14.1	652	45.1	740	1200	354	384	3183	95.6	329	4577	5.9	3.63	0.71345
Datong He @ Min He	CJ244	06/20/00	3504	8.47	18.3	707	53.8	641	1200	359	400	3011	99.2	320	4443	6.1	3.38	0.71310
Huang Shui @ Huang Yuan	CJ113	06/01/99	3359	8.71	9.2	1310	62.6	622	1510	871	406	3493	83.5	393	5637	8.2	4.40	0.71485
Huang Shui ab. Min He	CJ245	06/20/00	3031	8.20	21.7	3390	137	1410	3190	3160	3340	3015	142	868	12730	−1.0	11.3	0.71192
Internal Drainage																		
Nachiguole	CJ240	06/16/00	4489	7.99	17.8	2365	92.7	1060	964	1940	541	3059	149	436	6506	6.5	6.55	0.71135
Golmud	CJ241	06/17/00	4509	8.17	21.8	6160	136	1850	1020	4890	1435	3828	70.8	778	12040	3.7	10.7	0.71051
Qaidam @ Xiangride	CJ242	06/17/00	4316	8.31	22.0	3220	103	1430	1090	2690	920	3485	111	556	8363	4.2	9.03	0.71054
Qinghai Lake																		
S. Bank of Qinghai Lake	CJ243	06/18/00	3200	9.08	21.8	186000	4690	32200	1670	171000	33100	23220	2.9	16000	258400	−0.8	0.34	0.71154

[a] ab = above; bl = below; LB = left bank; RB = right bank; trib = tributary.
[b] Calculated mean elevation for individual drainage basins (Hearn et al., 2001).
[c] TDS = total dissolved solid = $Na + K + Mg + Ca + Cl + SO_4 + CO_3 + SiO_2$.
[d] TZ^{+} = total dissolved cations = $Na^{+} + K^{+} + 2Mg^{2+} + 2Ca^{2+}$ in μEq (10^{-6} charge equivalent units per L).
[e] NICB = net inorganic charge balance = $(TZ^{+} - TZ^{-})/TZ^{+} \times 100\%$, where $TZ^{-} = Cl^{-} + 2SO_4^{2-} + HCO_3^{-}$.

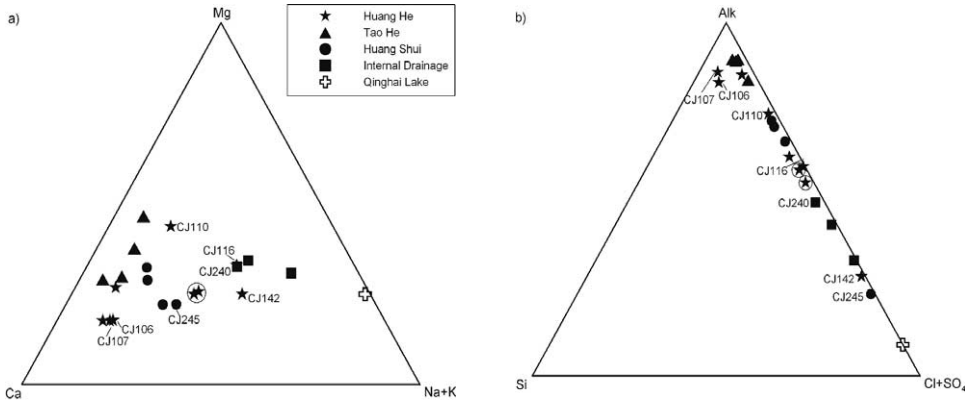

Fig. 3. (a) Cation and (b) anion ternary diagrams allow one to examine the chemical composition without the distraction of variable discharge or evaporation. Carbonate (Ca, Mg, Alk) and evaporite (Na + K, Cl + SO_4) are the dominant sources, and silicate (Si and also cations and Alk) a minor source of the dissolved load. These have been calculated in μEq units. Circled Huang He samples indicate the main channel at Lanzhou, our lowermost sample.

4.1.2. Carbonate weathering

Most samples are Ca-HCO_3 type, aside from the high-TDS samples, which we showed are Na-Cl type with significant SO_4 (Table 1). The calcite and dolomite saturation indices (CSI, DSI) calculated with the Geochemist's Workbench show that only Ka Chu and Mo Chu are undersaturated (Fig. 4). Other samples are supersaturated, as is common for natural waters in contact with $CaCO_3$ (Huh et al., 1998b; Dalai et al., 2002) due to inhibition of nucleation and precipitation of calcite by dissolved Mg^{2+}, PO_4^{3-}, or organic C (Inskeep and Bloom, 1986). We cannot provide definitive evidence for or against in situ $CaCO_3$ precipitation except to point out the absence of correlation between Ca/Sr ratio and CSI. Such a correlation can be evidence of selective removal of Ca by calcite precipitation (Jacobson et al., 2002), but the small range in Ca/Sr ratios in our own data set obscures any such relationship. The Qinghai Lake is significantly supersaturated with respect to dolomite (DSI of 5.9) compared to other samples (−0.3–3.4). This situation is in accord with the finding, though rare, of dolomite in its bottom sediments (Lister et al., 1991).

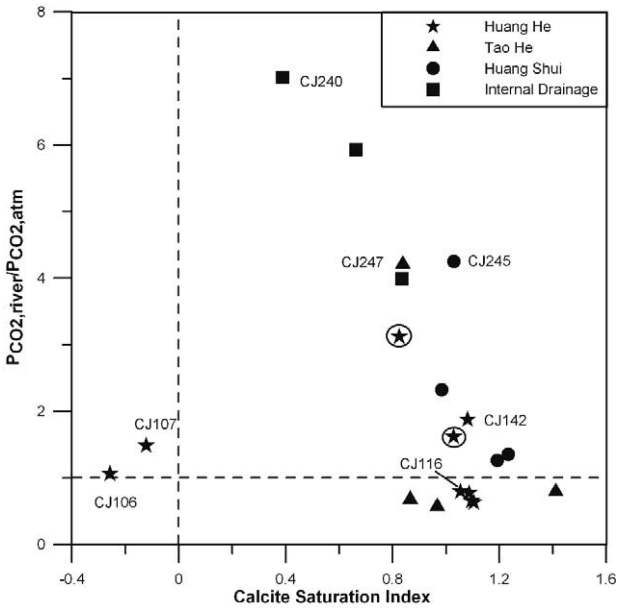

Fig. 4. $P_{CO2,rivers}/P_{CO2,atm}$ vs. calcite saturation index (CSI). CSI is defined as log ($\{Ca^{2+}\}\{CO_3^{2-}\}/K_{calcite}$) where {} denotes activity. The dolomite saturation index, log($\{Ca^{2+}\}\{Mg^{2+}\}\{CO_3^{2-}\}^2/K_{dolomite}$), has a similar trend (not shown). The dashed lines indicate saturation. The Upper Huang He samples are undersaturated to moderately supersaturated with respect to atmospheric CO_2, and hence not a substantial source of CO_2 emissions. The Qinghai Lake sample, omitted here, is supersaturated (CSI = 1.77, $P_{CO2,rivers}/P_{CO2,atm}$ = 1.8). Circled Huang He samples indicate the main channel at Lanzhou.

We computed saturation with respect to atmospheric CO_2, again using the Workbench. To correct for the effect of elevation on the partial pressure of atmospheric CO_2 (P_{CO2}), we employed the following equation (Andrews et al., 1996):

$$P_z = P_0 \exp(-Z/H) \quad (1)$$

where P_z is the partial pressure of CO_2 at altitude Z (km), P_0 is that at sea level (370 μatm), and H is the scale height (~8.4 km in the lower troposphere). For the Upper Huang He, we use P_4 (pressure at 4 km altitude) of 230 μatm. The high-TDS samples and those of the Huang Shui tributaries are supersaturated, while Tao He samples are undersaturated (Fig. 4). CJ247 is an exception and is supersaturated due to the lower pH (8.25). This range of supersaturation is commonly seen in other large rivers such as the Andean rivers of the Amazon (Stallard and Edmond, 1983; Richey et al., 1990), the Mackenzie (Kempe, 1982), and the Siberian rivers (Huh et al., 1998b). The excess CO_2 may be from the supersaturated soil pore waters that is flushed at high-water stage. In summary, thermodynamic evaluation of the data set indicates that the system is in contact with $CaCO_3$ and that CO_2 is perhaps added to the system through the decay of organic matter or dissolution of $CaCO_3$ accompanying pyrite oxidation.

4.1.3. Silicate weathering

Si concentrations can be a clear discriminator between carbonate and silicate weathering, an important distinction in terms of long-term uptake of atmospheric CO_2. However, Si is

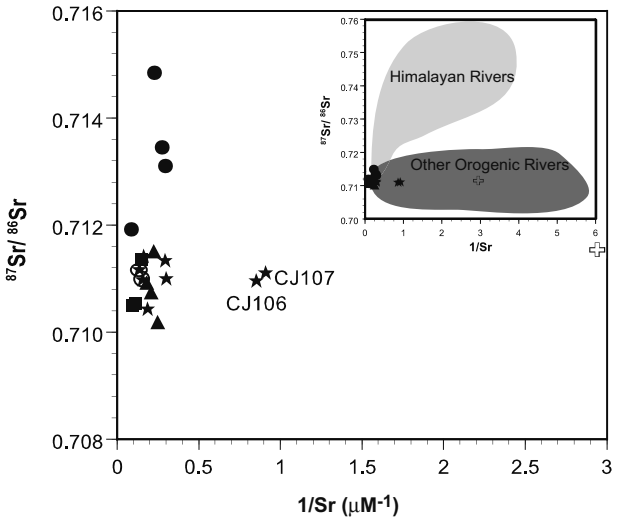

Fig. 5. $^{87}Sr/^{86}Sr$ vs. 1/Sr. The light grey envelope shows the range for Himalayan rivers (data source in the Introduction) and the dark grey envelope indicates the range for other orogenic zone rivers used for comparison. Symbols used are the same as in Figure 3.

involved in biogenic uptake by grass for phytolith production, or growth of diatoms in stagnant waters. Such reduction of Si (an extreme example in our data set is the Qinghai Lake) can be erroneously interpreted as lowering of silicate weathering rates. In the future, silicon isotope data may help to quantify this sink term, as preferential absorption of isotopically light Si by organisms would increase the $\delta^{30}Si$ values in the river-dissolved load (Ding et al., 2004). Alternatively, the low Si could be due to transformation between clay minerals that release Na or K but not Si, for example, muscovite to kaolinite.

4.1.4. *Strontium system*

The strontium concentration and isotope ratios range from 0.3 to 11 μM and from 0.710 to 0.715, respectively (Fig. 5). The most radiogenic values belong to the Huang Shui tributaries, and they lie on the trend of the Himalayan rivers (Fig. 5, inset). We suspect its source to be loess, based on the surficial coverage and the reported $^{87}Sr/^{86}Sr$ of ~0.714 of loess sections in Lanzhou (Yokoo et al., 2004) and in Xining (Jahn et al., 2001). The underlying Proterozoic to lower Paleozoic metamorphic rocks and granite in the Huang Shui drainage area could also contribute to high riverine $^{87}Sr/^{86}Sr$, but its rate of release is expected to be small due to the lack of extensive exposure and lower weathering rates. It is interesting that, even in an apparently carbonate-dominated terrain, we do not observe $^{87}Sr/^{86}Sr$ signature of marine carbonates, with ratios all above 0.710.

4.2. Inversion Calculation

4.2.1. *The model*

To quantify the relative contributions of carbonate, evaporite, and silicate lithologies to the dissolved load, and to calculate the drawdown of CO_2 by silicate weathering, we used an inversion model (Négrel et al., 1993). The model assumes that input from four sources—rain, evaporite dissolution, carbonate dissolution, and silicate weathering—can explain the dissolved major element and Sr isotope data. The set of mass balance equations are (Gaillardet et al., 1999)

$$\left(\frac{X}{Na}\right)_{river} = \sum_i \left(\frac{X}{Na}\right)_i \alpha_{i,Na} \quad (2)$$

$$\left(\frac{^{87}Sr}{^{86}Sr}\right)_{river}\left(\frac{Sr}{Na}\right)_{river} = \sum_i \left(\frac{^{87}Sr}{^{86}Sr}\right)_i \left(\frac{Sr}{Na}\right)_i \alpha_{i,Na} \quad (3)$$

where X stands for Ca, Mg, HCO_3, Cl, and Sr, i indicates the four source reservoirs (rain, evaporite, carbonate, silicate), and $\alpha_{i,Na}$ is the mixing proportion of sodium (Na) from the four reservoirs. To compensate for the variation in discharge and evaporative concentration, Na-normalized ratios and isotopic compositions are used instead of absolute content. Potassium (K) and SO_4 are excluded, because their geochemical cycles involve vegetation and bacterial activity, which may lead to nonconservative behavior during weathering (Berner and Berner, 1987). We weight the equations by analytical error for elemental ratios and $^{87}Sr/^{86}Sr$ ratios. Our model configuration is identical to that of Millot et al. (2003) except that we used a commercial Premium Solver optimization package with the Microsoft Excel spreadsheet program. We were able to reproduce their inversion results using their data and end members.

Starting from an a priori set of end-member compositions, $(X/Na)_i$, we iteratively solve for the proportion of those four end members in each sample ($\alpha_{i,Na}$) and the end-member compositions themselves, $(X/Na)_i$ (Table 2). Notice that we treat the end-member compositions as model parameters, recognizing the large uncertainties from sparse sampling of streams draining single lithologies. For the Upper Huang He dataset, all high-TDS samples are excluded because (1) the internal drainage rivers lie outside the Huang He, (2) mineral precipitation that may be active in these rivers is not taken into account in the inversion model, and (3) end-member compositions may be different for these extreme samples. We can use 15 samples, and thus we are solving for 75 model parameters (4 $\times$ 15 $\alpha_{i,Na}$ and 15 out of 24 $(X/Na)_i$) using 90 (6 $\times$ 15) mass balance equations and 15 constraining equations on the sum of fractions. The Global Optimization process within the Solver finds the solution that best predicts the measured compositions and $^{87}Sr/^{86}Sr$ ratios in the least-squares sense (Eqn. 2 and 3). Once the inversion model determines the best $\alpha_{rain,Na}$, $\alpha_{evap,Na}$, $\alpha_{carb,Na}$, and $\alpha_{sil,Na}$ for each sample, we use them to calculate these fractions for the rest of the elements considered (e.g., $\alpha_{rain,Ca}$, $\alpha_{evap,Ca}$, $\alpha_{carb,Ca}$, and $\alpha_{sil,Ca}$). We applied this model first to our own Upper Huang He data set and then to literature data on orogenic rivers. This enables us to compare the CO_2 drawdown rates hitherto estimated in diverse ways by various authors for different river systems.

4.2.2. *End-member designation*

We did not assume that one set of end members satisfies multiple river systems, but rather accommodated as much of the spatial variation in lithology as was practical. The philosophy was to use the end members proposed by the authors of the original literature, if available (see references listed in Table

Table 2. End-member composition ranges used in inversion calculations for the Upper Huang He and global orogenic rivers.

End member	Ca/Na	Mg/Na	HCO_3/Na	Cl/Na	1000 × Sr/Na	$^{87}Sr/^{86}Sr$
			Huang He[a]			
Rain	3.13	0.64	11.0	0.49	0.8–1.7	0.710
Evaporite	0.06–0.3	0.1–0.4	0.1–1.2	0.8–1.1	1–5	0.710–0.711
Carbonate	30–90	6–28	60–140	0.001	35–100	0.710–0.711
Silicate	0.2–0.5	0.12–0.36	1–3	0.001	2–3	0.72–0.80
			Mackenzie, Yukon, Siberian & Fraser[b]			
Rain (marine aerosol)	0.022	0.12	0.004	1.16	0.19	0.709
Evaporite (halite)	0.08–0.26	0.01–0.03	0–0.6	1	1–5	0.7076–0.7086
Carbonate (+gypsum)	30–70	12–28	60–140	0.001	50–100	0.708–0.709
Silicate	0.2–0.5	0.12–0.36	1–3	0.001	1–3	0.72–0.80
			Stikine & Fraser[c]			
Rain (marine aerosol)	0.022	0.12	0.004	1.16	0.19	0.709
Evaporite	0.08–0.26	0.01–0.03	0–0.6	1	1–5	0.703–0.704
Carbonate	30–70	12–28	60–140	0.001	50–100	0.703–0.704
Silicate	1.1–1.5	0.8–1.2	4–6	0.001	1–3	0.7045–0.7075
			Amazon & Orinoco[d]			
Rain	0.22–0.28	0.12–0.14	0.004	1.23–1.25	2–4	0.709
Evaporite	0.08–0.26	0.01–0.03	0–0.6	1	1–5	0.7076–0.7086
Carbonate	20–70	5–25	50–130	0.001	50–100	0.707–0.708
Silicate	0.2–0.8	0.3–0.7	1–3	0.001	3–7	0.72–0.74
			Yamuna & Ganga[e]			
Rain	2.2	0.61	6.8	0.74	8.5	0.7136
Evaporite	0.06–0.3	0.1–0.4	0.1–1.2	0.8–1.1	1.4–1.7	0.71
Carbonate	30–90	6–28	60–140	0.001	30–50	0.714–0.716
Silicate	0.4–1.0	0.1–0.5	1–3	0.001	1.2–2.9	0.78–0.82
			Ganges & Brahmaputra[f]			
Rain	2.2	0.61	6.8	0.74	8.5	0.7136
Evaporite	0.06–0.3	0.1–0.4	0.1–1.2	0.8–1.1	1.4–1.7	0.71
Carbonate	30–90	6–28	60–140	0.001	20–40	0.7079–0.72
Silicate	0.2	0.1–0.5	1–3	0.001	1.2–2.9	0.72–1.70
			Indus[g]			
Rain	2.2	0.61	6.8	0.74	8.5	0.7136
Evaporite	0.06–0.3	0.1–0.4	0.1–1.2	0.8–1.1	1.4–1.7	0.71
Carbonate	30–90	6–28	60–140	0.001	60–90	0.714–0.716
Silicate	0.4–1.0	0.1–0.5	1–3	0.001	1.2–2.9	0.76–0.80

[a] The rain end member is based on local rain in Xining and Golmud in 1988 (Zhang et al., 2003a), and the evaporite end member on Vengosh et al. (1995).
[b] Millot et al. (2003).
[c] Gaillardet et al. (2003). One sample of Fraser (FR114, Bridge) included.
[d] Modified from Gaillardet et al. (1997). Water data (no Sr) from Stallard and Edmond (1983) for the Amazon and from Edmond et al. (1996) for the Orinoco.
[e] End members from Krishnaswami et al. (1999). Water data from Dalai et al. (2002, 2003).
[f] End members and water data from Galy et al. (1999) and Galy and France-Lanord (1999).
[g] End members modified from Krishnaswami et al. (1999). Water data from Pande et al. (1994) and Karim et al. (2000).

2). At the same time, we carefully examined the data on property-property plots (Gaillardet et al., 1999) for individual river systems to fine-tune the end-member ranges. The a priori end-member compositions are given in terms of ranges in Na-normalized ratios, and the model iterates by varying the end members within these ranges (Table 2).

For the rain end member, commonly used sea-salt aerosol has been retained for all rivers under marine influence. The Upper Huang He lies in the continental interior, however, and we use local rainwater composition of Xining and Golmud cities (Zhang et al., 2003a) (Fig. 1b). This rain is alkaline (pH 6.9–8.2) due to weathering of calcite in the dust from local soil (Larssen and Carmichael, 2000; see section 4.2.3. for sensitivity of the model using other local rain values). The $^{87}Sr/^{86}Sr$ ratio of rain is estimated based on the water- and acetic acid-leachable portion of loess (0.71130 and 0.71073, respectively; Yokoo et al., 2004). The rain end members for the HTP rivers, the Amazon, and the Orinoco are based on local rain (Gaillardet et al., 1997; Galy and France-Lanord, 1999; Galy et al., 1999).

The range for the evaporite end member for global monolithologic rivers is not directly applicable to the Huang He, because borax, Na_2SO_4, $MgCl_2$, and KCl are found in addition to the common halite and gypsum. Instead, the evaporite end member is selected to encompass both the global end-member range and the chemical composition of input waters (Golmud River, Na-Mg-Cl type) to the salt lakes in the Qaidam Basin close to samples CJ240 and 241 (Vengosh et al., 1995). The Sr/Na ratio is low ($0.77–1.7 \times 10^{-3}$), and the Sr isotope ratio is based on the water-leachable part of the loess (Yokoo et al., 2004). The evaporite end members for the HTP rivers are modified from Galy and France-Lanord (1999) and Galy et al. (1999). For the Stikine we assumed a low $^{87}Sr/^{86}Sr$ similar to that of the carbonate end member (Gaillardet et al., 2003).

The carbonate end member is derived from a global collec-

Table 3. Rain end-member compositions used in sensitivity tests.

Scenarios	Location	Year	Ca/Na	Mg/Na	HCO_3/Na	1000 × Sr/Na	Cl/Na	$^{87}Sr/^{86}Sr$
1	Marine Aerosol		0.022	0.12	0.004	0.19	1.16	0.709
2	Xining & Golmud	1988	3.13	0.64	11.0	0.8–1.7	0.49	0.710
3	Xining & Golmud	1999/2000	1.63	0.20	5.53	0.8–1.7	0.51	0.710
4	Lhasa	1987/1988	0.84	0.032	3.25	0.8–1.7	0.24	0.710
5	Other Tibetan Towns	1987/1988	3.01	0.12	8.60	0.8–1.7	0.91	0.710
6	Range		0.84–3.13	0.032–0.64	3.25–11.0	0.8–1.7	0.24–0.91	0.710–0.712

tion of single-lithology rivers (Gaillardet et al., 1999). We assign slightly radiogenic and high-Sr values for the Huang He. This can be justified by the carbonate fraction of loess (~1000 ppm Sr) and of the bed load of the Huang He at Lanzhou (~800–6000 ppm Sr) (Asahara et al., 1999; Yokoo et al., 2004). HTP rivers also deviated from the global orogenic rivers with low Sr and high $^{87}Sr/^{86}Sr$ (Galy et al., 1999; Oliver et al., 2003) and Stikine with low $^{87}Sr/^{86}Sr$ of nonmarine or hydrothermal origin (Gaillardet et al., 2003).

The global silicate end member is modified for the Upper Huang He ($^{87}Sr/^{86}Sr$ 0.72 to 0.80), considering the silicate fraction of loess in the study area (0.71792–0.71975; Asahara et al., 1999; Yokoo et al., 2004) and granite in the Qilian mountains ($^{87}Sr/^{86}Sr$ of 0.80074) (Su et al., 2004). The silicate end member of the Stikine has higher Mg/Na and lower $^{87}Sr/^{86}Sr$ (Gaillardet et al., 2003). The end members for the HTP rivers are from the original authors.

4.2.3. Model uncertainty and sensitivity

As a first measure of uncertainty in our inversion model results, we propagated the analytical error (7% for concentrations and 0.00002 for $^{87}Sr/^{86}Sr$) according to the least-squares solution to the linearized Eqn. 2 and 3. This is a conservative estimate based on NICB, but the analytical error is usually <5%. The relative uncertainties for Na fractions from four reservoirs—$\alpha_{rain,Na}$, $\alpha_{evap,Na}$, $\alpha_{carb,Na}$, and $\alpha_{sil,Na}$—are on the order of 50%, 20%, 5%, and 40%, respectively. The propagated relative uncertainty for $\alpha_{sil,Cation}$ is ~30%.

We ran six scenarios to test the sensitivity of the a priori rain end members on $\alpha_{i,Cation}$ (Table 3). Our first scenario takes the marine aerosol composition. For our second scenario, we adopted the rain composition of two cities, Xining and Golmud, before development (Fig. 1b). The rainwater chemistry in these two cities corresponding to our sampling period 1999/2000 is used for the third scenario, which will probably be an overestimate as the rain samples were collected within the city. The fourth and fifth scenarios use 1987/1988 rain data of Lhasa and three other Tibetan towns, respectively (Zhang et al., 2003b). These stations are farther south of the Upper Huang He drainage basin but may be more representative of rural settings. In the sixth scenario, we treated the rain end member also as a model parameter, allowing it to vary within the range encompassing scenarios 2 to 5.

Scenario 2 is our best choice because (1) the rain stations are proximate to our sampling area; (2) it is more reflective of the unpolluted condition of our samples than scenario 3; and (3) the a posteriori end member of scenario 6 is similar to that of scenario 2. The evaporite and rain reservoirs were not distinguishable for our samples in the first scenario. Among the latter five scenarios, the second (Xining and Golmud 1988) and fourth (Lhasa 1987, Lhasa 1988) have the highest and lowest elemental ratios (X/Na) except for Cl, but no apparent relationship exists between $\alpha_{i,Cation}$ and the rain end-member compositions. The choice of end-member composition is very important to $\alpha_{sil,Cation}$, and a tributary of the Huang Shui (CJ112, CJ244) and the Huang He headwater (CJ116) are especially sensitive to the choice of the rain end member. The relative difference between the latter five scenarios for $\alpha_{sil,Cation}$ can be up to 130% (with average 70% and minimum 20%). This may be an overestimate because it includes rain in Lhasa, which is far from our drainage area. Indeed, the average relative difference for $\alpha_{sil,Cation}$ between scenarios 2 and 6 is 13% (0%–45%). In summary, if geologically informed selection of the a priori end members is made, the end-member compositions themselves are uniquely modeled, and a conservative estimate of the relative uncertainty on $\alpha_{sil,Cation}$ is ~30%.

4.2.4. Inversion results

The inversion result for the Upper Huang He shows that carbonate weathering supplies most of the dissolved load and that silicate weathering contribution is only minor. The Huang He subset, except the headwater (CJ116) and two Lanzhou samples, and the Tao He subset are dominated by carbonate weathering (50 to 89%)(Table 4). The major cations in the two Lanzhou samples are supplied by both evaporite and carbonate weathering. In the Huang Shui subset, there are similar proportions of rain, evaporite, and carbonate. The headwater sample (CJ116) has the highest evaporite component (70%) presumably due to the thin-bedded halite deposits in the area. The highest silicate fractions are found in two Huang He headwater tributaries (CJ106 and CJ107), which is consistent with their higher silica concentrations.

When we compare our inversion results with similar inversion calculations of Millot et al. (2003) and Gaillardet et al. (2003), the relative differences are 50 to 60%. This is mainly due to the samples used in inversion (only mountainous rivers vs. all). The relative differences between our inversion results and the forward budget model results of Dalai et al. (2002) and Galy and France-Lanord (1999) are 30 to 40%.

The following caveats should be considered when interpreting the inversion model results:

1. The source reservoirs are hypothetical and do not necessarily represent independent physical entities. Take the case of aeolian input: weathering of mineral dust by rainwater in the atmosphere, before contact with bedrock or sediments, is

Table 4. Inversion results and dissolved flux calculations for the Upper Huang He.

River name	Sample No.	Area	Runoff[a]	Discharge[b]	$Cation_{sil}$				Dissolved flux of cations			Net CO_2 yield
					Rain	Evaporite	Carbonate	Silicate	Evaporite	Carbonate	Silicate	$\emptyset Cation_{sil}$
		$10^3 km^2$	mm/yr	km^3/yr	%				10^9 mol/yr			10^3 mol/km^2/yr
Huang He												
Huang He @ Ma Doi	CJ116	21.21	90.9	1.93	21	70	7	2	5.34	0.56	0.13	6
Ka Chu @ Tang Ku	CJ106	6.024	570	3.43	10	5	62	24	0.09	1.24	0.47	78
Mo Chu @ Roergai	CJ107	2.719	419	1.14	28	1	50	20	0.01	0.42	0.17	62
LB trib. of Huang He	CJ115	2.783	170	0.472	9	21	67	3	0.21	0.66	0.03	11
Huang He bl. Tangnag	CJ114	122.8	225	27.6	3	12	75	10	5.54	33.9	4.52	37
RB trib. of Huang He	CJ110	5.188	171	0.889	0	19	67	13	0.37	1.28	0.25	49
Huang He @ Lanzhou	CJ111	231.6	172	39.9	7	49	30	14	69.2	42.3	20.4	88
Huang He @ Lanzhou	CJ246	231.6	172	39.9	1	46	35	18	67.1	52.0	26.9	116
Tao He Tributary												
Tao He headwaters	CJ108	6.703	275	1.84	0	9	85	6	0.23	2.20	0.16	24
LB trib. of Tao He	CJ109	1.578	230	0.363	0	10	81	9	0.05	0.42	0.05	30
Tao He @ Min Xian	CJ141	14.09	284	4.00	0	8	89	3	0.58	6.52	0.24	17
Tao He ab. Lin Tao	CJ247	19.68	243	4.78	0	9	79	12	0.89	7.86	1.18	60
Huang Shui Tributary												
Datong He @ Min He	CJ112	15.00	86.7	1.3	29	23	41	7	0.78	1.41	0.24	16
Datong He @ Min He	CJ244	15.00	86.7	1.3	33	23	34	10	0.77	1.17	0.32	21
Huang Shui @ Huang Yuan	CJ113	2.142	78.0	0.167	34	38	21	7	0.22	0.12	0.04	19

[a] Based on Fekete et al. (2002).
[b] Discharge data are calculated from runoff and drainage area. See text for data source.
ab. = above; bl. = below; LB = left bank; RB = right bank; trib = tributary.

treated as rain input. Weathering of dust that is introduced as dry deposition is incorporated into the three different lithologic reservoirs. The dust from the Taklimakan Desert dominates the total input of dust on the Qinghai-Tibet Plateau at ~100 g/m^2/yr (Zhang, 2001). Weathering of the silicate dust by CO_2 dissolved in the rain makes our estimation of CO_2 consumption rates (based only on silicate weathering and not rain) a minimum. On the other hand, if the agent of silicate weathering in the atmosphere is acid rain, our estimate is not affected. Disseminated calcite is another example. It is not explicitly included in the carbonate fraction, but to the extent that it is found in a wide variety of granites in general (White et al., 2005), we are implicitly including this in our silicate reservoir. Thus, if disseminated calcite is significant, we are overestimating the CO_2 drawdown by silicate weathering. For silicate terrain that has been exposed more than 1 yr, this becomes a moot point because long-term column experiment suggests that trace calcite will be exhausted after 1 yr (White et al., 2005).

2. Sink terms are not specifically addressed in the inversion model. Under semiarid conditions, precipitation of minerals is a viable process. We can only state that we do not find any positive proof that it is active (see section 4.1.2.).

3. Each reservoir is heterogeneous in its composition. For example, the Himalayan carbonates are lower in Sr concentrations and more radiogenic than elsewhere. Our solution was to assign different end members for different river systems, but we did not find it practical to do so within one river system. The evaporite end member is especially difficult to characterize because of the diversity of rock types in which they are found, and in the case of the Upper Huang He, because of the diversity of salt types. In addition, the similarity of the evaporite and marine aerosol compositions increases the uncertainties. Considering all these factors, we estimate that there is ~30% relative uncertainty on the $\alpha_{sil,Cation}$'s calculated.

4.3. Flux Calculations

We used ArcGIS software to calculate the drainage basin area and runoff for each sample using digital databases (Tables 4 and 5). Basin areas are modified from the USGS Global GIS database for South Asia (Hearn et al., 2001) and agree within 5% with those reported in literature (Li and Wu, 1999; Wang et al., 2004). Runoff data are from the UNEP/GRDC Composite Runoff Fields v 1.0, which is the interpolated runoff from those measured at hydrological stations (Fekete et al., 2002). We used a multiyear average based on stations with records longer than 12 yr and catchment areas greater than 2500 km^2. There were ~10 stations within 5° east or south of our study area that satisfied the conditions. The recorded natural discharge (at Lanzhou) is 33.6 km^3/yr averaged over 1955 to 1999 (Wang et al., 2002), and our estimated discharge for the main channel above Lanzhou is 39.9 km^3/yr. We used basin areas and mean annual discharge as given by the original author for other orogenic rivers (Table 6).

The TDS yield is ~10^6 mol/km^2/yr for most samples (Table 5). The high-TDS samples have moderate yield comparable to that of Huang He at Lanzhou, despite the extremely high concentrations, because the runoff is low. When broken down

Table 5. Dissolved flux calculations for the Upper Huang He.

River name	Area	Runoff	Discharge	Na	K	Mg	Ca	Cl	SO_4	HCO_3	Si	TDS flux	TDS yield	Net CO_2 yield 2ØSi
	10^3 km^2	mm/yr	km^3/yr				10^9 mol/yr					10^9 mol/yr	10^6 mol/km^2/yr	10^3 mol/km^2/yr
							Huang He							
Huang He @ Ma Doi	21.21	90.9	1.93	4.03	0.127	1.83	1.64	3.54	0.405	6.42	0.0505	18.0	0.851	4.77
Ka Chu @ Tang Ku	6.024	570	3.43	0.436	0.0559	0.310	1.20	0.0737	0.0833	3.06	0.381	5.59	0.928	126
Mo Chu @ Roergai	2.719	419	1.14	0.168	0.0272	0.129	0.505	0.0278	0.0222	1.29	0.137	2.30	0.846	101
LB trib. of Huang He	2.783	170	0.472	0.190	0.0152	0.156	0.628	0.133	0.233	1.05	0.0460	2.45	0.881	33.1
Huang He bl. Tangnag	122.8	225	27.6	7.56	0.778	11.0	25.8	3.17	3.04	68.7	2.66	123	1.00	43.2
RB trib. of Huang He	5.188	171	0.889	0.473	0.0414	0.720	0.672	0.215	0.293	2.50	0.0659	4.98	0.959	25.4
Huang He @ Lanzhou	231.6	172	39.9	65.0	1.95	27.2	48.3	40.3	21.2	121	4.19	330	1.42	36.2
Huang He @ Lanzhou	231.6	172	39.9	68.4	2.32	28.8	47.9	37.9	26.3	115	4.51	331	1.43	38.9
Wei He @ Wu Shan	8.069	66.5	0.536	2.38	0.0517	0.708	0.911	2.30	0.911	1.64	0.0600	8.96	1.11	14.9
							Tao He Tributary							
Tao He headwaters	6.703	275	1.84	0.309	0.0445	1.12	1.11	0.121	0.110	4.52	0.177	7.52	1.12	52.9
LB trib. of Tao He	1.578	230	0.363	0.0799	0.0102	0.180	0.252	0.0292	0.0240	0.870	0.0278	1.47	0.933	35.2
Tao He @ Min Xian	14.09	284	4.00	0.688	0.121	2.01	4.52	0.335	0.399	12.3	0.288	20.7	1.47	40.9
Tao He ab. Lin Tao	19.68	243	4.78	1.59	0.251	2.69	5.40	0.521	0.927	14.4	0.415	26.2	1.33	42.2
							Huang Shui Tributary							
Datong He @ Min He	15.00	86.7	1.30	0.848	0.0586	0.962	1.56	0.460	0.499	4.14	0.124	8.65	0.577	16.6
Datong He @ Min He	15.00	86.7	1.30	0.919	0.0699	0.833	1.56	0.467	0.520	3.91	0.129	8.41	0.561	17.2
Huang Shui @ Huang Yuan	2.142	78.0	0.167	0.219	0.0105	0.104	0.252	0.145	0.0678	0.583	0.0139	1.40	0.652	13.0
Huang Shui ab. Min He	15.26	69.1	1.05	3.56	0.144	1.48	3.35	3.32	3.51	3.17	0.149	18.7	1.22	19.5
							Internal Drainage							
Goldmud River	10.53	2.51	0.0264	0.0624	0.00245	0.0280	0.0254	0.0512	0.0143	0.0808	0.00393	0.269	0.0255	0.747
Qaidam River @ Xiangride	13.90	106	1.47	9.06	0.200	2.72	1.50	7.19	2.11	5.63	0.104	28.5	2.05	15.0

ab. = above; bl. = below; LB = left bank; RB = right bank; trib. = tributary.

Table 6. Comparison for rivers draining various orogenic belts in the world.

River name	Basin area[a]	Mean elevation[b]	Mean local relief[b]	Mean annual temperature[b]	Mean annual precipitation[b]	Mean annual runoff	TDS yield	Net CO_2 yield	Net CO_2 yield	References
	10^3 km^2	m	m	°C	mm/yr	mm/yr	10^6 mol/km^2/yr	$\varnothing Cation_{sil}$ 10^3 mol/km^2/yr	$2\varnothing Si$ 10^3 mol/km^2/yr	
Upper Huang He	231.6	3648	1600	1–8	430	172	0.56–1.5	6–116	5–126	Millot et al., 2003;
Mackenzie	181	1000–2500	272	−4	1000–1500	200–1700	0.50–4.9	5–57	9–99	Summerfield and
Yukon	166	1000–2500	504	−5	380	250–370	0.89–1.6	28–29	54–150	Hulton, 1994; Meybeck
Fraser	57.2	1140	n.a.	4	760	400–1200	0.54–2.9	9–211	62–143	and Ragu, 1997;
Siberian Rivers	1622	600–700	294	−9	~250	30–380	0.04–0.38	4–26	7–75	Edmond and Huh,
Stikine	90.7	1500–2000	n.a.	0–5	1500–1750	700–1300	0.72–1.3	82–108	51–69	1997; Pinet and
Orinoco	277	3000–7000	347	25	>2000	560–2000	0.96–1.6	145–234	208–290	Souriau, 1988; Stallard
Amazon	2082	3000–7000	215	27	>2000	780–2100	0.59–4.1	102–347	238–549	and Edmond, 1983;
Ganges	1060	100–5000	438	18	2030	430–1100	1.7–5.7	111–572	182–412	Huh et al., 1998a;
Brahmaputra	583	2734	992	15	2030	1050	1.7–2.2	164–196	325–537	Gaillardet et al., 2003;
Indus	470	4200	785	19	640	~500	1.3	162	35	Galy and France-Lanord, 1999; Dalai et al., 2002; Pande et al., 1994; Karim and Veizer, 2000; this study

[a] Basin area is for the mountainous rivers only.
[b] For entire basins including nonmountainous areas. The Siberian rivers are for the Lena only.

by elements, Ca and HCO_3 dominate the dissolved flux of the Upper Huang He (Table 5).

The consumption rate of CO_2 by silicate weathering is computed as the flux of total dissolved cations that came from silicate weathering:

$$\varnothing CO_2 = \varnothing Cation_{sil} = \varnothing (Na^+_{sil} + K^+_{sil} + Ca^{2+}_{sil} + Mg^{2+}_{sil}) \quad (4)$$

where Ø indicates yield (mol/km^2/yr). The premise for Eqn. 4 is that chemical weathering is equivalent to the ion exchange reaction between protons from hydrated atmospheric CO_2 and cations in the rock or sediment. Uptake of CO_2 by carbonate weathering is not included because it is not a net sink of atmospheric CO_2 on timescales longer than 1 my; the reaction reverses upon deposition of $CaCO_3$ in the ocean, releasing one mol of CO_2 back to the atmosphere per mol of Ca or Mg. The Na^+_{sil}, Ca^{2+}_{sil}, and Mg^{2+}_{sil} are outputs from the inversion model, and K flux is assumed to be solely from silicates ($\varnothing K^+_{river} = \varnothing K^+_{sil}$). Addition of K from salt and fertilizers is not taken into account, but considering that there is also removal by crop production and fixing by biomass, the error related to this assumption will be small. Excluding K affects the $\varnothing CO_2$ less than 30%, except for the Huang He headwater (CJ116), one mainstream sample (CJ115), and one Tao He sample (CJ141). The propagated relative uncertainty of $\varnothing CO_2$ is ~40% from the ~30% error for both $\alpha_{sil,Cation}$ and the discharge.

In the absence of quantified silicate-originating cation concentrations (from inversion calculations, for example), one has to resort to using $\varnothing CO_2 = 2\varnothing Si$ (Edmond and Huh, 1997). This estimate is based on groundwaters in igneous and metamorphic terrain whose Si/HCO_3^- ratios are generally 0.3 to 0.5 (Garrels, 1967). We calculated the net CO_2 consumption rates using $\varnothing CO_2 = \varnothing Cation_{sil}$ from inversion modeling and $\varnothing CO_2 = 2\varnothing Si$ relationship (Tables 4 and 5). These two sets of $\varnothing CO_2$ values obtained by two different methods give coherent results and passed a statistical paired-samples *t*-test at 5% significance level for the Huang He, but for other orogenic rivers (Table 6), the silica-based method gave higher $\varnothing CO_2$ than the inversion model at the 5% significance level. The Si/HCO_3^- ratio used may be watershed-dependent and may cause the discrepancy.

The consumption of atmospheric CO_2 by silicate weathering in the Upper Huang He ranges from 6×10^3 mol/km^2/yr in the evaporite-dominant headwater (CJ116) to 116×10^3 mol/km^2/yr at Lanzhou, our lowermost sampling point (Table 4). The CO_2 consumption rates are relatively high in the Ka Chu, Mo Chu, and one Tao He sample (CJ247), consistent with their relatively high $\alpha_{sil,Cation}$, but low in other samples ($6–49 \times 10^3$ mol/km^2/yr). That the two Lanzhou samples have the highest $\varnothing CO_2$ suggests that we are missing a high $\varnothing CO_2$ source. Since Huang He up to Tangnag (CJ114) and other tributaries have only moderate $\varnothing CO_2$, we think that the main channel between Tangnag and Lanzhou is responsible.

4.4. Upper Versus Lower Reaches

Examination of published data for the Huang He at its mouth shows that the TDS flux and yield vary ~12% interannually. Potassium and silica are especially variable (up to 40%); other major ion compositions vary <20% (Table 7). The major element composition of the middle and lower reaches is

Table 7. Comparison of the Upper Huang He with previous studies.

Reference	Location	Date	pH	Na μM	K μM	Mg μM	Ca μM	Cl μM	SO_4 μM	Alk μEq	Si μM	TDS[a] mg/l	TDS Yield 10^3 mol/km^2/yr	TDS Flux 10^9 mol/yr
This study	Upper reach @ Lanzhou	May-June, 1999 & 2000	8.47	1670	53.5	702	1205	981	596	2967	109	382	1427	331
Hu et al., 1982	Lower reach @ Sanmeng Dam	Oct. 1978	n.a.	2120	61.9	903	1249	1134	760	3700	95	464	646	375
SCOPE/UNEP	River mouth	July 1981	8.19	2257	81	642	931	1249	705	2580	233	389	433	325
SCOPE/UNEP	River mouth	July 1982	8.08	3140	119	865	935	1520	730	3640	166	488	554	416
Zhang et al., 1990	River mouth	May 1985	8.13	n.a.	n.a.	728	1048	1323	746	2984	n.a.	416[b]	n.a.	n.a.
Zhang et al., 1995	River mouth	Aug. 1986	8.26	2430	70	900	930	1260	900	3220	350	463	502	399

[a] TDS = total dissolved solid = Na + K + Mg + Ca + Cl + SO_4 + CO_3 + SiO_2.
[b] TDS does not include Si.
n.a. = data not available.

broadly similar to that of the upper part, showing mainly carbonate and evaporite weathering and minor silicate weathering. However, Na, K, and SO_4 concentrations are higher because of the agricultural, industrial, and mining activities.

The Upper Huang He supplies ~80% of the TDS flux at the mouth of the Huang He, whereas its drainage basin area is only ~22%. The TDS yield (normalized by area) is therefore ~3 times higher. Overall fluxes are similar, but there are differences in chemical composition because anthropogenic input adds specific elements to the main channel downstream.

4.5. Comparison to Rivers in Other Orogenic Zones

In terms of the major element composition, the Upper Huang He bears closest resemblance to the Mackenzie, both dominated by carbonate and evaporite weathering and having low $\emptyset CO_2$ (5–120 × 10^3 mol/km^2/yr). Silicate weathering becomes more important in other orogenic rivers, especially the Amazon, Orinoco, and the HTP rivers (100–570 × 10^3 mol/km^2/yr). The Huang He and the HTP rivers, even though they drain the same Himalaya-Tibetan Plateau system, differ significantly in their silicate weathering rates and uptake of atmospheric CO_2. The Indus, Ganges, and Brahmaputra are higher in Si and $^{87}Sr/^{86}Sr$ (0.715–1.24 vs. 0.710–0.715), and the CO_2 drawdown (110–570 × 10^3 mol/km^2/yr) is also higher than in the Upper Huang He (6–120 × 10^3 mol/km^2/yr; Table 6; Fig. 6). The Himalayan front has experienced high-grade metamorphism, while the eastern Tibetan Plateau has seen only the low-grade variety. Hence, while both the Huang He and the HTP rivers display carbonate dominance in the dissolved major element composition, the $^{87}Sr/^{86}Sr$ ratios are higher in the metamorphic carbonates of the Himalayan front, resulting from metamorphic remobilization of radiogenic Sr into calc-silicates (Edmond, 1992). This is reflected in the $^{87}Sr/^{86}Sr$ ratios of the headwaters of the Ganges, which among all other HTP rivers, seem to be uniquely driving the increased ^{87}Sr delivery to the oceans in the Cenozoic (Denison et al., 1998).

To apply the spatially and temporally spotty sampling of rivers to interpretations of a general nature regarding chemical weathering, we need to elucidate the fundamental relationships. There are three major factors influencing chemical weathering rates (physical erosion rates, runoff, and temperature) (West et al., 2005), and here we will test the latter two. The Arrhenius relationship is commonly used to describe the effect of temperature on silicate weathering rates, with the understanding that this can only be an empirical description tool when applied to watershed fluxes involving multiple mineral dissolution reactions and complex hydrochemical processes (White and Blum, 1995):

$$\text{Rate} = Ae^{-Ea/RT} \quad (5)$$

where E_a is the apparent activation energy (in kJ/mol), R is the gas constant, T is temperature (in Kelvin) and A is the preexponential factor. For the Upper Huang He, the correlation coefficient (R^2) is 0.23 if using $\emptyset CO_2 = \emptyset Cation_{sil}$ and 0.03 if using $\emptyset CO_2 = 2\emptyset Si$. From the slope of the regression line, the apparent activation energy is 48 kJ/mol ($\emptyset CO_2 = \emptyset Cation_{sil}$) and 18 kJ/mol ($\emptyset CO_2 = 2\emptyset Si$). There is a large disagreement between the two, because the total range of temperature is small

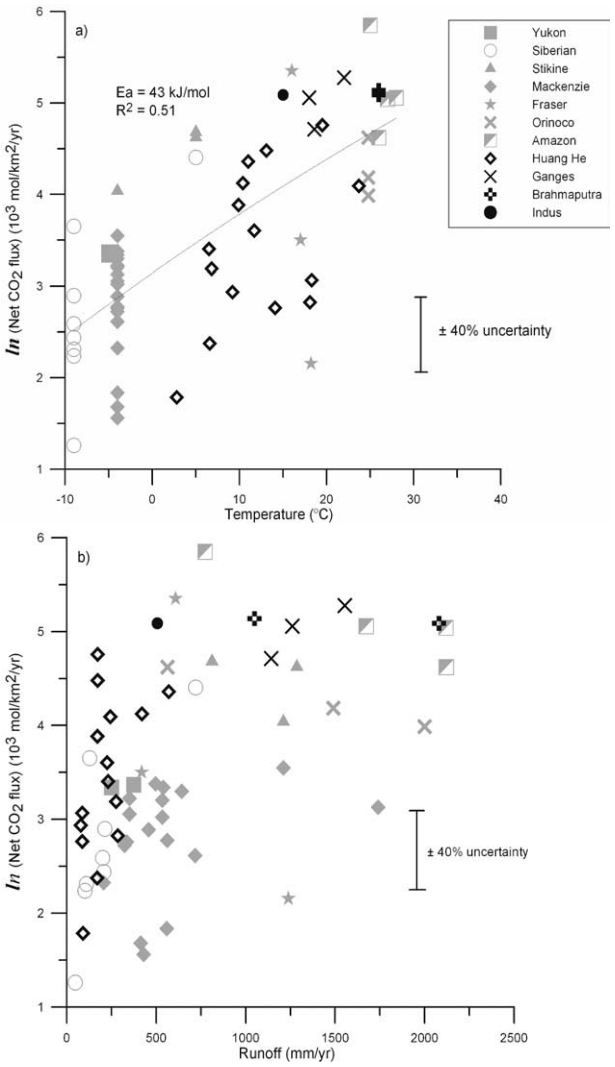

Fig. 6. (a) Arrhenius fit to net CO_2 yields (calculated using the $ØCO_2 = ØCation_{sil}$ relationship) and resulting apparent activation energy (E_a), and correlation coefficient (R^2). Water temperature measured in the field is used for the Upper Huang He, Fraser, and Amazon, and average annual air temperature for other rivers (Meybeck and Ragu, 1997; Gaillardet et al., 2003). (b) Net CO_2 flux vs. runoff.

and the number of samples is also small, making the least squares fit poor. Data for all orogenic-zone rivers yield an E_a of 43 kJ/mol ($ØCO_2 = ØCation_{sil}$) with R^2 of 0.51 (Fig. 6a) and an E_a of 40 kJ/mol ($ØCO_2 = 2ØSi$) with R^2 of 0.45. These values are close to those for basalt weathering (42.3 kJ/mol; Dessert et al., 2001), but lower than that for Ca-Mg-silicate weathering assumed in the GEOCARB model (62.8 kJ/mol; Berner and Kothavala, 2001) or for natural feldspar weathering (77.0 kJ/mol; Velbel, 1993). The lower E_a implies a smaller change in weathering rates for a given temperature variation. For example, when temperature changes from 0 to 25°C, the relative rate increases by 0.15% for an E_a of 40 kJ/mol and by 0.22% for an E_a of 60 kJ/mol. We interpret the lower E_a as implying weaker coupling between temperature and weathering rates than had been assumed.

The net CO_2 drawdown does not show a linear relationship with runoff (Fig. 6b). At low to moderate runoff, they show a positive relationship, but above ~800 mm/yr CO_2 uptake rates are independent of runoff. Two Mackenzie samples and one Fraser sample fall off the trend with lower CO_2 fluxes at a given runoff. In orogenic zones, the CO_2 drawdown is a function of both runoff and temperature, and it is difficult to resolve their effects because of the complicated lithology.

5. CONCLUSIONS

We investigated the dissolved major element and $^{87}Sr/^{86}Sr$ composition of the Upper Huang He draining the semiarid Qinghai-Tibet Plateau and found that carbonate and evaporite weathering provide the majority of solute flux with minor contribution from silicate weathering (<24%). In the Plateau interior, a few extremely saline (Na-Cl type) and alkaline rivers are supersaturated with respect to carbonate. The inversion model we used to calculate the contributions of rain, evaporite, carbonate, and silicate is sensitive to the end-member designation. We estimate the relative uncertainty to be, at best 20%, and more conservatively, ~40%. The Upper Huang He has higher chemical weathering rates per unit area than the basin as a whole. Compared with the Ganges draining the Himalayas, it has less radiogenic Sr and lower CO_2 uptake rates by silicate weathering, which we attribute to the paucity of highly radiogenic metamorphic calc-silicates and to lower runoff. The CO_2 drawdown in the Upper Huang He is higher than that in the Mackenzie, Yukon, and Siberian rivers. In large orogenic river systems, we find that CO_2 uptake rates are weakly coupled to temperature, and the dependence on runoff breaks down at high runoff values.

Acknowledgments—We thank the Chengdu Institute of Geology and Mineral Resources for logistical support in the field, A. Ellis for valuable discussion, T. Bullen for access to TIMS, and undergraduate students K. Harmon, K. Lee, and S. Holsinger for help in the lab. Y. Huh is indebted to C. Burchfiel and J. M. Edmond for providing fieldwork opportunities in China. We thank J. Gaillardet and two anonymous reviewers and associate editor S. Krishnaswami for their thoughtful comments. This work was supported by NSF OCE 9911416.

Associate editor: S. Krishnaswami

REFERENCES

Andrews J. E., Brimblecombe P., Jickells T. D., and Liss P. S. (1996) *An Introduction to Environmental Chemistry.* Blackwell Science.

Asahara Y., Tanaka T., Kamioka H., Nishimura A., and Yamazaki T. (1999) Provenance of the north Pacific sediments and process of source material transport as derived from Rb-Sr isotopic systematics. *Chem. Geol.* **158,** 271–291.

Berner E. K. and Berner R. A. (1987) *The Global Water Cycle: Geochemistry and Environment.* Prentice-Hall.

Berner R. A. and Kothavala Z. (2001) GEOCARB III: A revised model of atmospheric CO_2 over Phanerozoic time. *Am. J. Sci.* **301,** 182–204.

Bethke C. M. (2002) *The Geochemist's Workbench 4.0.*

Calmels D., Gaillardet J., Brenot A., and France-Lanord C. (2004) sulfur isotopes in the rivers of the Mackenzie River Basin: Implication for CO_2 consumption. *Eos Trans. AGU* **85,** Fall Meet. Suppl., # H43C-0386 (abstract).

Cameron E. M., Hall G. E. M., Veizer J., and Krouse H. R. (1995) Isotopic and elemental hydrogeochemistry of a major river system: Fraser River, Br. Columbia, Canada. *Chem. Geol.* **122,** 149–169.

Carbon Cycle Research Unit. (1982) The amount of carbon transported to the sea by the Yangtze and Huanghe Rivers (People's Republic

of China) during the half-year July-December, 1981. In *Transport of Carbon and Minerals in Major World Rivers. Part 1,* Vol. 52 (ed. E. T. Degens), pp. 437–448. Mittelungen aus dem Geologisch-Palaeontologischen Institut der Universitaet Hamburg.

Chen J., He D., and Cui S. (2003) The response of river water quality and quantity to the development of irrigated agriculture in the last 4 decades in the Yellow River Basin, China. *Water Resour. Res.* **39,** 1047.

Dalai T. K., Krishnaswami S., and Sarin M. M. (2002) Major ion chemistry in the headwaters of the Yamuna river system: Chemical weathering, its temperature dependence and CO_2 consumption in the Himalaya. *Geochim. Cosmochim. Acta* **66,** 3397–3416.

Dalai T. K., Krishnaswami S., and Kumar A. (2003) Sr and $^{87}Sr/^{86}Sr$ in the Yamuna River System in the Himalaya: sources, fluxes and controls on Sr isotope composition. *Geochim. Cosmochim. Acta* **67,** 2931–2948.

Denison R. E., Koepnick R. B., Burke W. H., and Hetherington E. A. (1998) Construction of the Cambrian and Ordovician seawater $^{87}Sr/^{86}Sr$ curve. *Chem. Geol.* **152,** 325–340.

Dessert C., Dupré B., François L. M., Schott J., Gaillardet J., Chakrapani G., and Bajpai S. (2001) Erosion of Deccan Traps determined by river geochemistry: impact on the global climate and the $^{87}Sr/^{86}Sr$ ratio of seawater. *Earth Planet. Sci. Lett.* **188,** 459–474.

Ding T., Wan D., Wang C., and Zhang F. (2004) Silicon isotope compositions of dissolved silicon and suspended matter in the Yangtze River, China. *Geochim. Cosmochim. Acta* **68,** 205–216.

Edmond J. M. (1992) Himalayan tectonics, weathering processes and the strontium isotope record in marine limestones. *Science* **258,** 1594–1597.

Edmond J. M. and Huh Y. (1997) Chemical weathering yields from basement and orogenic terrains in hot and cold climates. In *Tectonic Uplift and Climate Change* (ed. W. F. Ruddiman), pp. 329–351, Plenum Press.

Edmond J. M., Palmer M. R., Measures C. I., Brown E. T., and Huh Y. (1996) Fluvial geochemistry of the eastern slope of the northeastern Andes and its foredeep in the drainage of the Orinoco in Colombia and Venezuela. *Geochim. Cosmochim. Acta* **60,** 2949–2974.

Fekete B., Vörösmarty C. J., and Grabs W. (2002) High-resolution fields of global runoff combining observed river discharge and simulated water balances. *Global Biogeochem. Cycles* **16,** doi: 10.1029/1999GB001254.

Gaillardet J., Dupre B., Allegre C. J., and Negrel P. (1997) Chemical and physical denudation in the Amazon River Basin. *Chem. Geol.* **142,** 141–173.

Gaillardet J., Dupré B., Louvat P., and Allègre C. J. (1999) Global silicate weathering and CO_2 consumption rates deduced from the chemistry of large rivers. *Chem. Geol.* **159,** 3–30.

Gaillardet J., Millot R., and Dupré B. (2003) Chemical denudation rates of the western Canadian orogenic belt: the Stikine terrane. *Chem. Geol.* **201,** 257–279.

Galy A. and France-Lanord C. (1999) Weathering processes in the Ganges-Brahmaputra basin and the riverine alkalinity budget. *Chem. Geol.* **159,** 31–60.

Galy A., France-Lanord C., and Derry L. A. (1999) The strontium isotopic budget of Himalayan rivers in Nepal and Bangladesh. *Geochim. Cosmochim. Acta* **63,** 1905–1925.

Gan W.-B., Chen H.-M. and Han Y.-F. (1983) Carbon transport by the Yangtze (at Nanjing) and Huanghe (at Jinan) Rivers, People's Republic of China. In *Transport of Carbon and Minerals in Major World Rivers. Part 2,* Vol. 55 (ed. E. T. Degens, S. Kempe and H. Soliman), pp. 459–470. Mittelungen aus dem Geologisch-Palaeontologischen Institut der Universitaet Hamburg.

Garrels R. M. (1967) Genesis of some groundwaters from igneous rocks. In *Researches in Geochemistry,* Vol. 2 (ed. P. H. Abelson), pp. 405–420, John Wiley.

Han Y.-R. (2002) Development and protection of water resources in the source region of the three rivers. *J. Changjiang Vocational Univ.* **19,** 12–15 (in Chinese with English abstract).

Hearn P. P., Jr., Hare T. M., Schruben P., Sherrill D., LaMar C., and Tsushima P. (2001) *Global GIS Database: Digital Atlas of South Asia.* U.S. Geological Survey.

Hu M.-H., Stallard R. F., and Edmond J. M. (1982) Major ion chemistry of some large Chinese rivers. *Nature* **298,** 550–553.

Huh Y., Panteleyev G., Babich D., Zaitsev A., and Edmond J. M. (1998a) The fluvial geochemistry of the rivers of Eastern Siberia: II. Tributaries of the Lena, Omoloy, Yana, Indigirka, Kolyma and Anadyr draining the collisional/accretionary zone of the Verkhoyansk and Cherskiy ranges *Geochim. Cosmochim. Acta* **62,** 2053–2075.

Huh Y., Tsoi M.-Y., Zaitsev A., and Edmond J. M. (1998b) The fluvial geochemistry of the rivers of Eastern Siberia: I. Tributaries of the Lena River draining the sedimentary platform of the Siberian Craton *Geochim. Cosmochim. Acta* **62,** 1657–1676.

Inskeep W. P. and Bloom P. R. (1986) Kinetics of calcite precipitation in the presence of water-soluble organic ligands. *Soil Sci. Soc. Am. J.* **50,** 1167–1172.

Jacobson A. D., Blum J. D., and Walter L. M. (2002) Reconciling the elemental and Sr isotope composition of Himalayan weathering fluxes: Insights from the carbonate geochemistry of stream waters. *Geochim. Cosmochim. Acta* **66,** 3417–3429.

Jahn B.-M., Gallet S., and Han J. (2001) Geochemistry of the Xining, Xifeng and Jixian sections, Loess Plateau of China: eolian dust provenance and paleosol evolution during the last 140 ka. *Chem. Geol.* **178,** 71–94.

Jiang Z., Gao Q., Liu S., and Ren Z. (1997) Research on sulfide atmosphere transport in China and East-Asia areas - statistical transport model of stream fields classification. *Res. Env. Sci.* **10,** 14–21 (in Chinese with English abstract).

Jones B. F. and Deocampo D. M. (2003) Geochemistry of saline lakes. In *Treatise on Geochemistry: Surface and Groundwater, Weathering and Soils,* Vol. 5 (ed. J. I. Drever), pp. 365–392, Elsevier.

Karim A. and Veizer J. (2000) Weathering processes in the Indus River Basin: implications from riverine carbon, sulfur, oxygen and strontium isotopes. *Chem. Geol.* **170,** 153–177.

Kempe S. (1982) Long-term records of CO_2 pressure fluctuations in fresh waters. In *Transport of Carbon and Minerals in Major World Rivers. Part 1* Vol. 52 (ed. E. T. Degens), pp. 91–332. Mittelungen aus dem Geologisch-Palaeontologischen Institut der Universitaet Hamburg.

Krishnaswami S., Singh S. K. and Dalai T. K. (1999) Silicate weathering in the Himalaya: Role in contributing to major ions and radiogenic Sr to the Bay of Bengal. In *Ocean Science, Trends and Future Directions* (ed. B. L. K. Somayajulu), pp. 23–51, Indian National Science Academy and Akademia International.

Lan Y.-C., Kang E.-S., Ma Q.-J., Yang W.-H., and Yao Z.-Z. (1999) Runoff forecast model for inflow to the Longyangxia Reservoir in the upper Yellow River basin during spring. *J. Glaciol. Geocryol.* **21,** 391–395.

Larssen T. and Carmichael G. R. (2000) Acid rain and acidification in China: the importance of base cation deposition. *Environ. Pollut.* **110,** 89–102.

Li L., Zhang G., Qang Q., and Shi X. (2000) Study on evapotranspiration and its impact factors over Yellow River upper stream area. *Adv. Earth Sci.* **15,** 256–259 (in Chinese with English abstract).

Li W. and Wu G. (1999) Source and composition of water and sediment in upper reaches of the Yellow River in Qinghai Province. *Bull. Soil Water Conservat.* **19,** 6–10 (in Chinese with English abstract).

Lister G. S., Kelts K., Zao C. K., Yu J.-Q., and Niessen F. (1991) Lake Qinghai, China: closed-basin lake levels and the oxygen isotope record for ostracoda since the latest Pleistocene. *Palaeogeog. Palaeoclimat. Palaeoecol.* **84,** 141–162.

Meybeck M. (1979) Concentrations des eaux fluviales en éléments majeurs et apports en solution aux océans. *Rev. Géol. Dyn. Géogr. Phys.* **21,** 215–246.

Meybeck M. and Ragu A. (1997) *River Discharges to the Oceans: An Assessment of Suspended Solids, Major Ions and Nutrients.* UNEP Publication.

Millot R., Gaillardet J., Dupré B., and Allègre C. J. (2003) Northern latitude chemical weathering rates: Clues from the Mackenzie River Basin, Canada. *Geochim. Cosmochim. Acta* **67,** 1305–1329.

Ministry of Public Security. (1993) *Population Data by County and City*. Ministry of Public Security, Beijing, P.R.C.

Négrel P., Allègre C. J., Dupré B., and Lewin E. (1993) Erosion sources determined by inversion of major and trace element ratios and strontium isotopic ratios in river water; the Congo Basin case. *Earth Planet. Sci. Lett.* **120,** 59–76.

Oliver L., Harris N., Bickle M., Chapman H., Dise N., and Horstwood M. (2003) Silicate weathering rates decoupled from the $^{87}Sr/^{86}Sr$ ratio of the dissolved load during Himalayan erosion. *Chem. Geol.* **201,** 119–139.

Pande K., Sarin M. M., Trivedi J. R., Krishnaswami S., and Sharma K. K. (1994) The Indus river system (India-Pakistan): Major-ion chemistry, uranium and strontium isotopes. *Chem. Geol.* **116,** 245–259.

Peng X., Wu Q.-B., and Tian M.-Z. (2003) The effect of groundwater table lowering on ecological environment in the headwaters of the Yellow River. *J. Glaciol. Geocryol.* **25,** 667–671 (in Chinese with English abstract).

Pinet P. and Souriau M. (1988) Continental erosion and large-scale relief. *Tectonics* **7,** 563–582.

Raymo M. E. and Ruddiman W. F. (1992) Tectonic forcing of late Cenozoic climate. *Nature* **359,** 117–122.

Richey J. E., Hedges J. I., Devol A. H., Quay P. D., and Victoria R. (1990) Biogeochemistry of carbon in the Amazon River. *Limnol. Oceanogr.* **35,** 352–371.

Stallard R. F. and Edmond J. M. (1983) Geochemistry of the Amazon 2. The influence of geology and weathering environment on the dissolved load. *J. Geophys. Res.* **88,** 9671–9688.

Su J., Hu N., Zhang H., and Feng B. (2004) U-Pb zircon dating and genesis of the Heigouliangzi granitic intrusion in the western segment of the middle Qilian mountains. *Geoscience* **18,** 70–74 (in Chinese with English abstract).

Su X., Lin X., Liao Z., and Wang J. (2001) The evaporation effect on the isotopes in the Yellow River water. *J. Geosci. Res. Northeastern Asia* **4,** 178–184.

Summerfield M. A. and Hulton N. J. (1994) Natural controls of fluvial denudation rates in major world drainage basins. *J. Geophys. Res.* **99,** 1319.

Sun D., Chen F., Bloemendal J., and Su R. (2003) Seasonal variability of modern dust over the Loess Plateau of China. *J. Geophys. Res.* **108,** doi:10.1029/2003JD003382.

Sun H. (1992) A general review of volcanogenic massive sulphide deposits in China. *Ore Geol. Rev.* **7,** 43–71.

Sun J. (2002) Provenance of loess material and formation of loess deposits on the Chinese Loess Plateau. *Earth Planet. Sci. Lett.* **203,** 845–859.

Tapponnier P., Peltzer G., and Armijo R. (1986) On the mechanics of the collision between India and Asia. *Geol. Soc. Spec. Publ.* **19,** 115–157.

Velbel M. A. (1993) Temperature dependence of silicate weathering in nature: How strong a negative feedback on long-term accumulation of atmospheric CO_2 and global greenhouse warming? *Geology* **21,** 1059–1062.

Vengosh A., Chivas A. R., Starinsky A., Kolodny Y., Baozhen Z., and Pengxi Z. (1995) Chemical and boron isotope compositions of nonmarine brines from the Qaidam Basin, Qinghai, China. *Chem. Geol.* **120,** 135–154.

Wang B. and Lin H. (2002) Rainy season of the Asian-Pacific summer monsoon. *J. Climate* **15,** 386–397.

Wang B., Clemens S. C., and Liu P. (2003) Contrasting the Indian and East Asian monsoons; implications on geologic timescales. *Mar. Geol.* **201,** 5–21.

Wang Y.-M., Zhang X.-C., Wang L., and Zhou J.-B. (2002) Analysis of changes in natural runoff in the Yellow River basin in 1990. *Yellow River* **24,** 9–11 (in Chinese with English abstract).

Wang Y.-Z., Kang L.-L., and Wang G.-Q. (2004) Precipitation variations happened in the upper stream of the Yellow River and effects to its runoff in the last 50 years. *Yellow River* **26,** 5–7 (in Chinese with English abstract).

Wen X.-Q., Yang G.-H., Wang D.-X., and Ren G.-X. (2004) Vegetation compartmentalization in source regions of Yangtse River and Yellow River. *J. Northwest Sci.-Tech. Univ. Agri. For. (Nat. Sci. Ed.)* **32,** 5–8.

West A. J., Galy A., and Bickle M. (2005) Tectonic and climatic controls on silicate weathering. *Earth Planet. Sci. Lett.* **235,** 211–228.

White A. F. and Blum A. E. (1995) Effects of climate on chemical weathering in watersheds. *Geochim. Cosmochim. Acta* **59,** 1729–1747.

White A. F., Schulz M. S., Lowenstern J. B., Vivit D. V., and Bullen T. D. (2005) The ubiquitous nature of accessory calcite in granitoid rocks: Implications for weathering, solute evolution and petrogenesis. *Geochim. Cosmochim. Acta* **69,** 1455–1471.

Yan J. P., Hinderer M., and Einsele G. (2002) Geochemical evolution of closed-basin lakes: general model and application to Lakes Qinghai and Turkana. *Sediment. Geol.* **148,** 105–122.

Yang D., Li C., Hu H., Lei Z., Yang S., Kusuda T., Koike T., and Musiake K. (2004) Analysis of water resources variability in the Yellow River of China during the last half century using historical data. *Water Resour. Res.* **40,** doi:10.1029/2003WR002763.

Yang Q. (1989) Borate deposits in Qaidam Basin. *Acta Sedim. Sinica* **7,** 117–123 (in Chinese with English abstract).

Yang S.-L., Zhao Q.-Y., and Belkin I. M. (2002) Temporal variation in the sediment load of the Yangtze river and the influences of human activities. *J. Hydrol.* **263,** 56–71.

Yang Z., Cheng Y., and Wang H. (1986) *The Geology of China.* Clarendon Press, Oxford.

Yokoo Y., Nakano T., Nishikawa M., and Quan H. (2004) Mineralogical variation of Sr-Nd isotopic and elemental compositions in loess and desert sand from the central Loess Plateau in China as a provenance tracer of wet and dry deposition in the northwestern Pacific. *Chem. Geol.* **204,** 45–62.

Zhang D. D., Jim C. Y., Peart M. R., and Shi C. (2003a) Rapid changes of precipitation pH in Qinghai Province, the northeastern Tibetan Plateau. *Sci. Total Environ.* **305,** 241–248.

Zhang D. D., Peart M., Jim C. Y., He Y. Q., Li B. S., and Chen J. A. (2003b) Precipitation chemistry of Lhasa and other remote towns, Tibet. *Atmos. Environ.* **37,** 231–240.

Zhang J., Huang W. W., Liu M. G., and Zhou Q. (1990) Drainage basin weathering and major element transport of two large Chinese rivers (Huanghe and Changjiang). *J. Geophys. Res.* ***95****, 13,277-* **13,** 28819.

Zhang J., Huang W. W., Létolle R., and Jusserand C. (1995) Major element chemistry of the Huanghe (Yellow River), China –- weathering processes and chemical fluxes. *J. Hydrol.* **168,** 173–203.

Zhang S.-Q., Wang Y.-G., Zhao Y.-Z., Huang Y., Li Y.-G., Shi W.-D., and Shang X.-G. (2004) Permafrost degradation and its environmental impact in the source regions of the Yellow River. *J. Glaciol. Geocryol.* **26,** 1–6 (in Chinese with English abstract).

Zhang X. (2001) Source distributions, emission, transport, deposition of Asian dust and loess accumulation. *Quat. Sci.* **21,** 29–40 (in Chinese with English abstract).

Zheng M. (1997) *An Introduction to Saline Lakes on the Qinghai-Tibet Plateau.* Kluwer Acadamic Publisher, Dordrecht.